Entropy generation for peristaltic motion of Carreau's fluid with mixture of ethylene glycol and boron-nitride nanoparticles

M Gul[1], F M Abbasi[1], Sabir A Shehzad[2] and Ahmad Shafee[3,4]

[1] Department of Mathematics, COMSATS University Islamabad, Islamabad 44000, Pakistan
[2] Department of Mathematics, COMSATS University Islamabad, Sahiwal 57000, Pakistan
[3] FAST, University Tun Hussein Onn Malaysia, 86400, Parit Raja, Batu Pahat, Johor State, Malaysia
[4] Public Authority of Applied Education & Training, College of Technological Studies, Applied Science Department, Shuwaikh, Kuwait

E-mail: sabirali@cuisahiwal.edu.pk

CrossMark

Abstract
Present work addresses the mixed convective peristaltic transport of electrically conducting ethylene glycol and boron-nitride nanofluids through inclination of asymmetric channel. This investigation also includes the effects of Hall and Ohmic heating. The factor of thermal conductivity is considered to change with temperature. Computations have been done for entropy, temperature, velocity, pressure gradient and concentration by considering the lubrication theory. Analytical solutions of nonlinear system have been computed through homotopy perturbation method. Entropy generation is analyzed graphically under Brownian movement, variable conductivity and thermophoresis aspects. Numeric benchmark of heat mass transport rates is presented. Stresses at the boundaries are examined using bar charts. This research shows that the studied nanofluid presents rise in entropy generation for increase in Hall parameter while reduction is noted when thermal and concentration Grashoff numbers increases. Entropy generation can be controlled at the upper wall when inclination of channel increases but at the same time it rises at the lower wall. Also, the results are found to be in good agreement with the numerical and outcomes reported previously.

Keywords: entropy generation, peristaltic flow, EG-BN nanofluid, variable thermal conductivity, Ohmic heating

(Some figures may appear in colour only in the online journal)

Nomenclature

$(\bar{x}, \bar{y})$	dimensional coordinates in wave frame	$\bar{t}$	dimensional time parameter
$(\bar{u}, \bar{v})$	dimensional velocity component in wave frame	$\bar{Q}$	dimensional flow rate in laboratory frame
		$\bar{q}$	dimensional flow rate in wave frame
d	half width of the channel	$\bar{S}_{ij}$	components of stress tensor
(h_1, h_2)	non-dimensional walls in wave frame	$\bar{A}_1$	Rivlin–Erickson tensor
(a, b)	amplitudes of the wave	F	dimensionless flow rate in wave frame
c	wave velocity	D_B	Brownian diffusion coefficient
n	dimensionless power law index	D_T	thermophoresis diffusion coefficient
		K	thermal conductivity

B_0	applied magnetic field
L	gradient of velocity
(T_m, C_m)	mean temperature and concentration
N_s	entropy generation number
B_e	Bejan number
Pr	Prandtl number
Bi	heat transfer Biot-number
Mi	mass transfer Biot-number
W_e	Weissenberg number
Br	Brinkman number
Ec	Eckert number
M	Hartmann number
N_t	thermophorosis parameter
N_b	Brownian motion parameter
G_t	thermal Grashoff number
G_c	concentration Grashoff number

Greek symbols

β	viscosity parameter
α	fluid parameter
μ	dimensionless flow rate
σ_f	electrical conductivity
η	apparent viscosity
ψ	stream function
ϕ	dimensionless concentration
θ	dimensionless temperature
$\dot{\gamma}$	shear rate
ϵ	phase difference
ω^*	concentration coefficient
α^*	thermal expansion Coefficient
ω	inclination angle
λ	wavelength
δ	wave number

1. Introduction

Nanofluids are essential for thermal efficiency improvement and are considered for commercial applications. Nanofluids revealed finer heat transfer characteristics than conventional fluids and are being extensively used in biomedicines, industrial and engineering processes such as cryosurgery, hyperthermia, IT cooling, nuclear power plants, microelectronics, building heating, milk pasteurization etc [1–8]. Dogonchi *et al* [9] presented the effect of non-uniform heat source on MHD of nanofluid over expanding flat. Reduction in concentration profile is seen with rising of the heterogeneous and homogenous reaction parameters. Furthermore, shape effects of nanoparticles are studied to determine the

heat transfer [10]. Moreover, the role of natural convection between a wavy circular cylinder and rhombus is investigated to analyze heat transfer of Fe_3O_4–*water* nanofluid [11].

Peristalsis is well known for its numerous implications in industrial and physiological systems. Food transport, blood circulation, transport of urine etc are some physiological applications which occur because of the contraction and expansion of flexible walls. Moreover, peristalsis in connection with heat transfer is beneficial for corrosive fluid transport, analysis of tissues, hemodialysis and oxygenation etc. Further, the notion of mass transfer is important in metal sanitization, blood purification in kidneys, water and salt absorption in plants and nuclear reactors etc. Several studies related to peristalsis can be visualized through [12–15].

Advancement in technology of flow meters, power plants, hydroelectric, radar systems, blood pump machines, Bleeding reduction during surgeries and heating elements etc make the study of MHD very important. MHD coupled with peristalsis of nanofluids is considered beneficial for drug delivery, detection of tumor and treating cancer tissues etc. In view of such frequent applications peristaltic flows have been investigated by various investigators (see [16–19]).

Non-Newtonian fluids have been demonstrated to be very significant in several fields. Rheological properties of fluids can be predicted through Carreau's fluid which is one of the models suggested for non- Newtonian fluids. In-spite of change in thermal properties, mechanical properties can also be affected by the incorporation of nanoparticles in fluid. Such rheological properties of nanofluids can be well predicted when the nanofluid is assumed to be non-Newtonian in nature. Rheological properties of ethylene glycol-boron nitride nanofluids are presented by Zyla *et al* [20]. In this study authors showed experimentally that EG-BN nanofluid exhibits non-Newtonian nature and proposed that the Carreau's fluid model can be used to predict the rheological characteristics of BN-EG nanofluid. Investigation on such fluids has been pursued by number of researchers for different models [21–24].

In recent years, analysis of entropy generation has gained popularity among researchers because of its association with real processes. Entropy generation occurs where the quality of energy decreases due to the disorder in system. Such disorder or randomness is mainly caused by process specially heat transfer. Improvement in the heat transfer processes due to the development in the advance fluids such as nanofluid, more the chances of energy lose. Hence distribution of entropy generation is important to be analyzed within the fluid volume in order to preserve quality of energy. The minimization of entropy generation is used for controlling and estimating the blood flow in arteries during hyperthermia, optimization of thermal engineering devices such as solar collector, electronic cooling devices etc. Some investigations in this direction can be found through [25–31]. Some studies display rise in entropy generation number as the Rayleigh number and the nanoparticles volume fraction increase [32, 33]. Seyyedi *et al* [34] reported the numerical results of a research on entropy generation for convective hydromagnetic flow in inclined cavity. Their results showed decay in entropy generation

number for constant Rayleigh and increasing Hartmann numbers.

Analyzing entropy generation for peristalsis of BN-EG nanofluid with variable thermal conductivity has not been presented so far. To include rheological aspects for Carreau's fluid, Buongiornio's formulation has been employed where important slip mechanisms i.e. Brownian diffusion and thermophoresis effects are incorporated. This paper presents a detailed study of such flow under influence of magnetic field through asymmetric channel. Final equations have been solved analytically via homotopy perturbation method (HPM). It is worth stating that the method is applied without limiting assumption and is free of round-off errors. Unlike perturbation method which requires small parameter in the equation.

2. Mathematical modeling

Consider the peristaltic flow of boron-nitride nanoparticles suspended in ethylene-glycol mixture in an asymmetric inclined channel of thickness $(d_1 + d_2)$. The channel's length is taken parallel to $\overline{X}$-axis and $\overline{Y}$-axis is chosen normal to it. Further, the channel is inclined at an angle ω. Due to a magnetic field $B(=(0, 0, B_0))$, Hall effect and Ohmic dissipation aspects are included. Two dimensional velocity field is considered to be of the form $V = [\overline{U}(\overline{X}, \overline{Y}, \overline{t}), \overline{V}(\overline{X}, \overline{Y}, \overline{t}), 0)]$. The forms of waves propagating on the channel walls are defined as:

$$\overline{H}_1(\overline{X}, \overline{t}) = d_1 + a_1 \cos\left(\frac{2\pi}{\lambda}(\overline{X} - c\overline{t})\right)$$

$$\overline{H}_2(\overline{X}, \overline{t}) = -d_2 - b_1 \cos\left(\frac{2\pi}{\lambda}(\overline{X} - c\overline{t}) + \epsilon\right).$$

Here, $\overline{t}, \lambda, \epsilon$ represent the time, wavelength, phase difference of two waves and a_1, b_1 signifies the amplitude of waves at upper-lower walls, respectively. The equations governing the flow are presented as:

$$\frac{\partial \overline{U}}{\partial \overline{X}} + \frac{\partial \overline{V}}{\partial \overline{Y}} = 0, \tag{1}$$

$$\rho_f\left(\frac{\partial}{\partial \overline{t}} + \overline{U}\frac{\partial}{\partial \overline{X}} + \overline{V}\frac{\partial}{\partial \overline{Y}}\right)\overline{U} = -\frac{\partial \overline{P}}{\partial \overline{X}}$$
$$+ \left(\frac{\partial \overline{S}_{\overline{X}\overline{X}}}{\partial \overline{X}} + \frac{\partial \overline{S}_{\overline{X}\overline{Y}}}{\partial \overline{Y}}\right) - \frac{\sigma_f B_0^2}{1 + m^2}(\overline{U} - m\overline{V})$$
$$+ \rho_f g \alpha^*(T - T_m)\sin\omega$$
$$+ \rho_f g \omega^*(C - C_m)\sin\omega, \tag{2}$$

$$\rho_f\left(\frac{\partial}{\partial \overline{t}} + \overline{U}\frac{\partial}{\partial \overline{X}} + \overline{V}\frac{\partial}{\partial \overline{Y}}\right)\overline{V} = -\frac{\partial \overline{P}}{\partial \overline{Y}} + \left(\frac{\partial \overline{S}_{\overline{Y}\overline{X}}}{\partial \overline{X}} + \frac{\partial \overline{S}_{\overline{Y}\overline{Y}}}{\partial \overline{Y}}\right)$$
$$- \frac{\sigma_f B_0^2}{1 + m^2}(\overline{V} + m\overline{U}) - \rho_f g \alpha^*(T - T_m)\cos\omega$$
$$- \rho_f g \omega^*(C - C_m)\cos\omega, \tag{3}$$

$$(\rho C)_f\left(\frac{\partial}{\partial \overline{t}} + \overline{U}\frac{\partial}{\partial \overline{X}} + \overline{V}\frac{\partial}{\partial \overline{Y}}\right)T = \overline{\nabla}.[\overline{K}(T)(\overline{\nabla}T)]$$
$$+ \overline{S}.L + \frac{\sigma_f B_0^2}{1 + m^2}(\overline{U}^2 + \overline{V}^2) + \tau(\rho C)_f\left[D_B\left(\frac{\partial C}{\partial \overline{X}}\frac{\partial T}{\partial \overline{X}}\right.\right.$$
$$\left.\left. + \frac{\partial C}{\partial \overline{Y}}\frac{\partial T}{\partial \overline{Y}}\right) + \frac{D_T}{T_m}\left(\frac{\partial T}{\partial \overline{X}} + \frac{\partial T}{\partial \overline{Y}}\right)^2\right], \tag{4}$$

$$\left(\frac{\partial}{\partial \overline{t}} + \overline{U}\frac{\partial}{\partial \overline{X}} + \overline{V}\frac{\partial}{\partial \overline{Y}}\right)C = D_B\left(\frac{\partial^2 C}{\partial \overline{X}^2} + \frac{\partial^2 C}{\partial \overline{Y}^2}\right)$$
$$+ \frac{D_T}{T_m}\left(\frac{\partial^2 T}{\partial \overline{X}^2} + \frac{\partial^2 T}{\partial \overline{Y}^2}\right). \tag{5}$$

In these equations, $m\left(=\frac{\sigma_f B_0}{en_e}\right)$, $\overline{P}$, ρ_f, T and T_m denote the Hall parameter, pressure, density, fluid's temperature and the mean temperature of both the channel walls respectively. Further, $\overline{S}.L$ stands for the viscous dissipation term, L the velocity gradient, g represents the acceleration due to gravity, C the concentration, $\overline{S}_{ij}$ the extra stress tensor's components, ω^* the coefficient of concentration expansion, C_f the fluid's specific heat, α^* the thermal expansion coefficient and $\overline{K}(T)$ the dimensional thermal conductivity. Moreover, D_B and D_T indicate the mass diffusivity and thermal diffusivity respectively. Also, $\tau (= \frac{(\rho C)_p}{(\rho C)_f})$ is the ratio of effective heat capacity of nanoparticles to the heat capacity of base fluid.

Hence, an extra stress tensor of Carreau's fluid is stated as:

$$\overline{S} = \overline{A}_1\eta, \tag{6}$$

here η and $\overline{A}_1$ and represent the apparent viscosity and first Rivlin–Erickson tensor respectively. Where,

$$\eta = \left[\eta_\infty + \frac{\eta_0 - \eta_\infty}{(1 + (\alpha\dot{\gamma})^2)^{\frac{n}{2}}}\right], \tag{7}$$

here $\dot{\gamma}$ is defined as:

$$\dot{\gamma} = \sqrt{2trD^2}, D = \frac{1}{2}A_1 \text{ and } A_1 = \text{grad}V$$
$$+ (\text{grad}V)^T. \tag{8}$$

In the above relations the zero shear-rate and the infinite shear-rate viscosities are denoted by η_0 and η_∞. Further, α, grad V, $\dot{\gamma}$ and n denote the fluid parameter, the velocity gradient, the shear rate and the non-dimensional power law index.

The transformations for wave frames $(\overline{x}, \overline{y})$ and laboratory $(\overline{X}, \overline{Y}, \overline{t})$ are given as:

$$\overline{x} = \overline{X} - c\overline{t}, \overline{y} = \overline{Y}, \overline{v} = \overline{V}, \overline{u} = \overline{U} - c, \overline{p}(\overline{x}, \overline{y})$$
$$= \overline{P}(\overline{X}, \overline{Y}, \overline{t}). \tag{9}$$

By using above transformations in equations (1)–(5), one obtains:

$$\frac{\partial \overline{u}}{\partial \overline{x}} + \frac{\partial \overline{v}}{\partial \overline{y}} = 0, \tag{10}$$

$$\rho_f\left((\bar{u} + c)\frac{\partial}{\partial \bar{x}} + \bar{v}\frac{\partial}{\partial \bar{y}}\right)(\bar{u} + c) = -\frac{\partial \bar{p}}{\partial \bar{x}}$$

$$+ \left(\frac{\partial \bar{s}_{\bar{x}\bar{x}}}{\partial \bar{x}} + \frac{\partial \bar{s}_{\bar{x}\bar{y}}}{\partial \bar{y}}\right) - \frac{\sigma_f B_0^2}{1 + m^2}((\bar{u} + c) - m\bar{v})$$

$$+ \rho_f g\alpha^*(T - T_m)\sin\omega + \rho_f g\omega^*$$

$$\times (C - C_m)\sin\omega, \qquad (11)$$

$$\rho_f\left((\bar{u} + c)\frac{\partial}{\partial \bar{x}} + \bar{v}\frac{\partial}{\partial \bar{y}}\right)\bar{v} = -\frac{\partial \bar{p}}{\partial \bar{y}} + \left(\frac{\partial \bar{s}_{\bar{y}\bar{x}}}{\partial \bar{x}} + \frac{\partial \bar{s}_{\bar{y}\bar{y}}}{\partial \bar{y}}\right)$$

$$- \frac{\sigma_f B_0^2}{1 + m^2}(\bar{v} + m(\bar{u} + c)) - \rho_f g\alpha^*(T - T_m)\cos\omega$$

$$- \rho_f g\omega^*(C - C_m)\cos\omega, \qquad (12)$$

$$(\rho C)_f\left((\bar{u} + c)\frac{\partial}{\partial \bar{x}} + \bar{v}\frac{\partial}{\partial \bar{y}}\right)T = \left(\frac{\partial}{\partial \bar{x}} + \frac{\partial}{\partial \bar{y}}\right)$$

$$\times \left[\bar{K}(T)\left(\frac{\partial}{\partial \bar{x}} + \frac{\partial}{\partial \bar{y}}\right)T\right] + \bar{s}.L + \frac{\sigma_f B_0^2}{1 + m^2}$$

$$\times ((\bar{u} + c)^2 + \bar{v}^2) + \tau(\rho C)_f[D_B$$

$$\times \left(\frac{\partial C}{\partial \bar{x}}\frac{\partial T}{\partial \bar{x}} + \frac{\partial C}{\partial \bar{y}}\frac{\partial T}{\partial \bar{y}}\right) + \frac{D_T}{T_m}\left(\frac{\partial T}{\partial \bar{x}} + \frac{\partial T}{\partial \bar{y}}\right)^2, \qquad (13)$$

$$\left((\bar{u} + c)\frac{\partial}{\partial \bar{x}} + \bar{v}\frac{\partial}{\partial \bar{y}}\right)C = D_B\left(\frac{\partial^2 C}{\partial \bar{x}^2} + \frac{\partial^2 C}{\partial \bar{y}^2}\right)$$

$$+ \frac{D_T}{T_m}\left(\frac{\partial^2 T}{\partial \bar{x}^2} + \frac{\partial^2 T}{\partial \bar{y}^2}\right). \qquad (14)$$

Here $\bar{s}.L$ represents the viscous dissipation term. Also, the stress components $\bar{s}_{ij}$ for Carreau's model are given as:

$$\bar{s}_{\bar{x}\bar{x}} = 2\eta_0\left[1 + \frac{\alpha^2 n}{2}(\beta - 1)\{2\bar{u}_{\bar{x}}^2 + 2\bar{v}_{\bar{y}}^2 + (\bar{u}_{\bar{y}} + \bar{v}_{\bar{x}})^2\}\right]\bar{u}_{\bar{x}},$$

$$\bar{s}_{\bar{x}\bar{y}} = \eta_0\left[1 + \frac{\alpha^2 n}{2}(\beta - 1)\{2\bar{u}_{\bar{x}}^2 + 2\bar{v}_{\bar{y}}^2 + (\bar{u}_{\bar{y}} + \bar{v}_{\bar{x}})^2\}\right](\bar{u}_{\bar{y}} + \bar{v}_{\bar{x}}),$$

$$\bar{s}_{\bar{y}\bar{y}} = 2\eta_0\left[1 + \frac{\alpha^2 n}{2}(\beta - 1)\{2\bar{u}_{\bar{x}}^2 + 2\bar{v}_{\bar{y}}^2 + (\bar{u}_{\bar{y}} + \bar{v}_{\bar{x}})^2\}\right](\bar{v}_{\bar{y}}). \qquad (15)$$

The dependence of thermal conductivity of nanofluid on temperature is provided via relation:

$$\bar{K}(T) = K_0(1 + \xi_0(T - T_0)). \qquad (16)$$

Here ξ_0 represents the dimensional thermal conductivity parameter at constant temperature.

Making use of following dimensionless parameters and variables:

$$x = \frac{\bar{x}}{\lambda}, y = \frac{\bar{y}}{d_1}, u = \frac{\bar{u}}{c}, v = \frac{\bar{v}}{c\delta}, \delta = \frac{d_1}{\lambda}, t = \frac{c\bar{t}}{\lambda},$$

$$h_1 = \frac{\bar{H}_1}{d_1}, h_2 = \frac{\bar{H}_2}{d_1}, a = \frac{a_1}{d_1}, b = \frac{b_1}{d_1}, d = \frac{d_2}{d_1},$$

$$p = \frac{d_1^2 \bar{p}}{c\lambda\eta_0}, \upsilon = \frac{\eta_0}{\rho_f}, \xi = \xi_o T_o, s_{xy} = \frac{d_1 \bar{s}_{\bar{x}\bar{y}}}{\eta_0 c},$$

$$K(\theta) = \frac{\bar{K}(T)}{K_o}, M^2 = \frac{\sigma_f}{\eta_0}B_0^2 d_1^2, Re = \frac{\rho_f c d_1}{\eta_0},$$

$$Pr = \frac{\eta_0 C_f}{K_0}, Ec = \frac{c^2}{C_f(T_1 - T_0)}, \varphi = \frac{1}{1 + m^2},$$

$$\phi = \frac{C - C_m}{C_1 - C_0}, \theta = \frac{T - T_m}{T_1 - T_0}, Br = Pr.Ec,$$

$$N_t = \frac{\tau D_T(T_1 - T_0)}{\upsilon T_m}, N_b = \frac{\tau D_B(C_1 - C_0)}{\upsilon},$$

$$W_e = \frac{\alpha c}{d_1}, G_t = \frac{d_1^2 \rho_f g\alpha^*(T_1 - T_0)}{\eta_0 c},$$

$$G_c = \frac{d_1^2 \rho_f g\omega^*(C_1 - C_0)}{\eta_0 c}, u = \psi_y, v = -\psi_x \qquad (17)$$

and using the small Reynolds number and large wave length approximations, equation of continuity is satisfied identically and components of momentum equations i.e. x and y take following form:

$$\frac{\partial p}{\partial x} = \frac{\partial}{\partial y}\left[\left\{1 + \frac{n}{2}(\beta - 1)W_e^2\left(\frac{\partial^2 \psi}{\partial y^2}\right)^2\right\}\frac{\partial^2 \psi}{\partial y^2}\right]$$

$$- M^2\varphi\left(\frac{\partial \psi}{\partial y} + 1\right) + G_t\theta\sin\omega + G_c\phi\sin\omega, \qquad (18)$$

$$\frac{\partial p}{\partial y} = 0. \qquad (19)$$

Solving equations (18) and (19), one obtains the following form:

$$\frac{\partial^2}{\partial y^2}\left[\left\{1 + \frac{n}{2}(\beta - 1)W_e^2\left(\frac{\partial^2 \psi}{\partial y^2}\right)^2\right\}\frac{\partial^2 \psi}{\partial y^2}\right] - M^2\varphi\frac{\partial^2 \psi}{\partial y^2}$$

$$+ G_t\frac{\partial \theta}{\partial y}\sin\omega + G_c\frac{\partial \phi}{\partial y}\sin\omega = 0. \qquad (20)$$

4

Table 1. Heat and mass transfer rates at the upper wall for various parameters when $n = 2.5$, $W_e = 0.1$, $x = 0$, $Pr = 0.5$, $Br = 0.3$, $a = 0.4$, $b = 0.3$, $\mu = 0.7$, $M = 1$, $\epsilon = \frac{\pi}{4}$, $d = 0.8$, $\beta = \frac{0.052\,6613}{1.33}$, $\omega = \frac{\pi}{6}$.

ξ	ω	φ	G_c	G_t	N_b	N_t	$-\theta'(h_1)$	$-\phi'(h_1)$
0.0	$\pi/4$	0.5	2.0	2.0	0.5	0.5	0.783 36	0.028 78
0.2							0.872 72	−0.012 66
0.4							0.970 37	−0.054 12
0.2	0						0.928 68	−0.012 66
	$\pi/6$						0.872 72	−0.012 66
	$\pi/3$						0.831 75	−0.012 66
0.2	$\pi/4$	0.1					0.812 91	0.038 72
		0.4					0.857 82	0.000 17
		0.7					0.857 82	−0.038 36
0.2	$\pi/4$	0.5	0.0				0.900 70	−0.012 66
			1.5				0.879 71	−0.012 66
			3.0				0.858 73	−0.012 66
0.2	$\pi/4$	0.5	2.0	0.0			0.900 70	−0.012 66
				1.5			0.879 71	−0.012 66
				3.0			0.858 73	−0.01266
0.2	$\pi/4$	0.5	2.0	2.0	0.5		0.872 72	−0.012 66
					1.0		0.953 32	0.175 04
					1.5		1.038 23	0.237 61
0.2	$\pi/4$	0.5	2.0	2.0	0.5	0.5	0.872 72	−0.012 66
						1.0	0.970 43	−0.543 55
						1.5	1.076 78	−1.178 08

Table 2. Qualitative comparison of present study with the results of Abbasi *et al* [23].

φ	Velocity for present study	Velocity for previous study [23]	Temperature for present study	Temperature for previous study [23]	Concentration for present study	Concentration for previous study [23]
0	−0.168 301	0.159 052	0.228 039	0.624 138	−0.067 2404	−0.576 545
0.1	−0.170 642	0.155 116	0.237 224	0.690 52	−0.076 4253	−0.635 007
0.2	−0.172 939	0.151 262	0.246 353	0.756 246	−0.085 5541	−0.692 289

In these equations Pr, Br, Ec and M denote the Prandtl, Brinkman, Eckert and Hartman parameters, while W_e, G_t and G_c indicate the Weissenberg, thermal Grashof and concentration Grashof numbers respectively. The terms N_t, N_b and φ signify thermophoresis, Brownian motion and Hall parameters. In addition, ϕ is the concentration, θ the fluid's dimensionless temperature, ψ the stream function and C_m the mean concentration. The terms C_0, T_0 and C_1, T_1 are concentration and temperature of upper and lower walls respectively.

Dimensionless energy, concentration and stress tensor expressions in wave-frame reference under lubrication approach are:

$$\frac{\partial}{\partial y}\left[(1 + \xi\theta)\frac{\partial\theta}{\partial y}\right] + Br\phi + PrN_b\frac{\partial\phi}{\partial y}\frac{\partial\theta}{\partial y} + PrN_t\left(\frac{\partial\theta}{\partial y}\right)^2$$
$$+ BrM^2\varphi\left(\frac{\partial\psi}{\partial y} + 1\right)^2 = 0, \tag{21}$$

$$\frac{\partial^2\phi}{\partial y^2} + \left(\frac{N_t}{N_b}\right)\frac{\partial^2\theta}{\partial y^2} = 0, \tag{22}$$

$$s_{xy} = s_{yx} = \left\{1 + \frac{n}{2}(\beta - 1)W_e^2\left(\frac{\partial^2\psi}{\partial y^2}\right)^2\right\}\frac{\partial^2\psi}{\partial y^2}.$$

Here $\beta\left(=\frac{\eta_\infty}{\eta_0}\right)$ is the viscosity parameter and ϕ in above equation is given as:

$$\phi = \left[1 + \frac{n}{2}(\beta - 1)W_e^2\left(\frac{\partial^2\psi}{\partial y^2}\right)^2\right]\left(\frac{\partial^2\psi}{\partial y^2}\right)^2,$$

and dimensionless walls are given as:

$$h_1(x) = 1 + a\cos(2\pi x),$$
$$h_2(x) = -d - b\cos(2\pi x + \epsilon).$$

Dimensionless no slip conditions are given as:

$$\psi = \frac{F}{2}, \frac{\partial\psi}{\partial y} = -1, \phi = -\frac{1}{2}, \theta = -\frac{1}{2} \text{ at } y = h_1,$$
$$\psi = -\frac{F}{2}, \frac{\partial\psi}{\partial y} = -1, \phi = \frac{1}{2}, \theta = \frac{1}{2} \text{ at } y = h_2. \tag{23}$$

Relationship between dimensionless volume flow rate in laboratory and wave frames $\mu\left(=\frac{\overline{Q}}{cd}\right)$ and $F\left(=\frac{\overline{q}}{cd}\right)$ are stated

as:

$$\mu = F + 1 + d. \tag{24}$$

Here, dimensional flow rate in fixed and moving frames are represented by $\overline{Q}$ and $\overline{q}$ respectively, where F is given as:

$$F = \int_{h_2}^{h_1} \frac{\partial \psi}{\partial y} dy. \tag{25}$$

The dominance of heat transfer irreversibility can be analyzed through Bejan which is defined as the ratio of heat transfer entropy generation to the total entropy generation. It is given as:

$$Be = \frac{N_h}{N_s}.$$

Dimensionless form of Bejan number is given as:

$$Be = \frac{(1 + \xi\theta)\left(\frac{\partial\theta}{\partial y}\right)^2}{(1 + \xi\theta)\left(\frac{\partial\theta}{\partial y}\right)^2 + Br\phi + BrM^2\varphi\left(\frac{\partial\psi}{\partial y} + 1\right)^2 + PrN_b\frac{\partial\phi}{\partial y}\frac{\partial\theta}{\partial y} + PrN_t\left(\frac{\partial\theta}{\partial y}\right)^2}. \tag{30}$$

3. Entropy generation

Entropy generation equation is written in a form:

$$S_G = \frac{\overline{K}(T)}{(T_1 - T_0)^2}\{(\overline{\nabla}T)^2\} + \frac{1}{(T_1 - T_0)}[\overline{s}.L] + \frac{1}{(T_1 - T_0)}$$

$$\times \left[\frac{\sigma_f B_0^2}{1 + m^2}(\overline{U}^2 + \overline{V}^2)\right] + \frac{1}{(T_1 - T_0)}[\tau(\rho C)_f$$

$$\times \left[D_B\left(\frac{\partial C}{\partial \overline{X}}\frac{\partial T}{\partial \overline{X}} + \frac{\partial C}{\partial \overline{Y}}\frac{\partial T}{\partial \overline{Y}}\right) + \frac{D_T}{T_m}\left(\frac{\partial T}{\partial \overline{X}} + \frac{\partial T}{\partial \overline{Y}}\right)^2\right]. \tag{26}$$

Here S_G indicates the actual entropy and its ratio to the characteristic entropy generation is termed as entropy generation number which is denoted by N_s and is expressed as:

$$N_s = \frac{S_G}{S_c}. \tag{27}$$

Here S_c stands for characteristic entropy generation and it is defined as:

$$S_c = \frac{K_0}{d_1^2}. \tag{28}$$

Dimensionless form of entropy generation after utilizing equations (8) and (16) due to the heat transfer, viscous dissipation, magnetic field, Brownian motion and thermophoresis effects is given as:

$$N_s = (1 + \xi\theta)\left(\frac{\partial\theta}{\partial y}\right)^2 + Br\phi + BrM^2\varphi\left(\frac{\partial\psi}{\partial y} + 1\right)^2$$

$$+ PrN_b\frac{\partial\phi}{\partial y}\frac{\partial\theta}{\partial y} + PrN_t\left(\frac{\partial\theta}{\partial y}\right)^2. \tag{29}$$

4. Analytical method

The system presented through expressions (20)–(22) having boundary condition (23) is solved using HPM. The above equations are written as follows:

$$H(\psi, p) = (1 - p)[L_1(\psi) - L_1(\psi_0)]$$

$$+ p\left[L_1(\psi) + \frac{\partial^2}{\partial y^2}\left[\left\{\frac{n}{2}(\beta - 1)W_e^2\left(\frac{\partial^2\psi}{\partial y^2}\right)^2\right\}\frac{\partial^2\psi}{\partial y^2}\right]\right.$$

$$\left. - M^2\varphi\frac{\partial^2\psi}{\partial y^2} + G_t\frac{\partial\theta}{\partial y}\sin\omega + G_c\frac{\partial\phi}{\partial y}\sin\omega\right], \tag{31}$$

$$H(\theta, p) = (1 - p)[L_2(\theta) - L_2(\theta_0)]$$

$$+ p\left[L_2(\theta) + \frac{\partial}{\partial y}\left[(\xi\theta)\frac{\partial\theta}{\partial y}\right] + Br\phi + PrN_b\frac{\partial\phi}{\partial y}\frac{\partial\theta}{\partial y}\right.$$

$$\left. + PrN_t\left(\frac{\partial\theta}{\partial y}\right)^2 + BrM^2\varphi\left(\frac{\partial\psi}{\partial y} + 1\right)^2\right], \tag{32}$$

$$H(\phi, p) = (1 - p)[L_3(\phi) - L_3(\phi_0)]$$

$$+ p\left[L_3(\phi) + \left(\frac{N_t}{N_b}\right)\frac{\partial^2\theta}{\partial y^2}\right]. \tag{33}$$

The linear operators are selected as follows:

$$L_1 = \frac{\partial^4}{\partial y^4}, \tag{34}$$

$$L_2 = \frac{\partial^2}{\partial y^2}, \tag{35}$$

$$L_3 = \frac{\partial^2}{\partial y^2}. \tag{36}$$

And the initial guesses are defined as:

$$\psi_0 = -\frac{(h_1 + h_2 - 2y)(-2(h_1 - h_2)(h_1 - y)(h_2 - y) + F(h_1^2 - 4h_1h_2 + h_2^2 + 2(h_1 + h_2)y - 2y^2))}{2(h_1 - h_2)^3}, \tag{37}$$
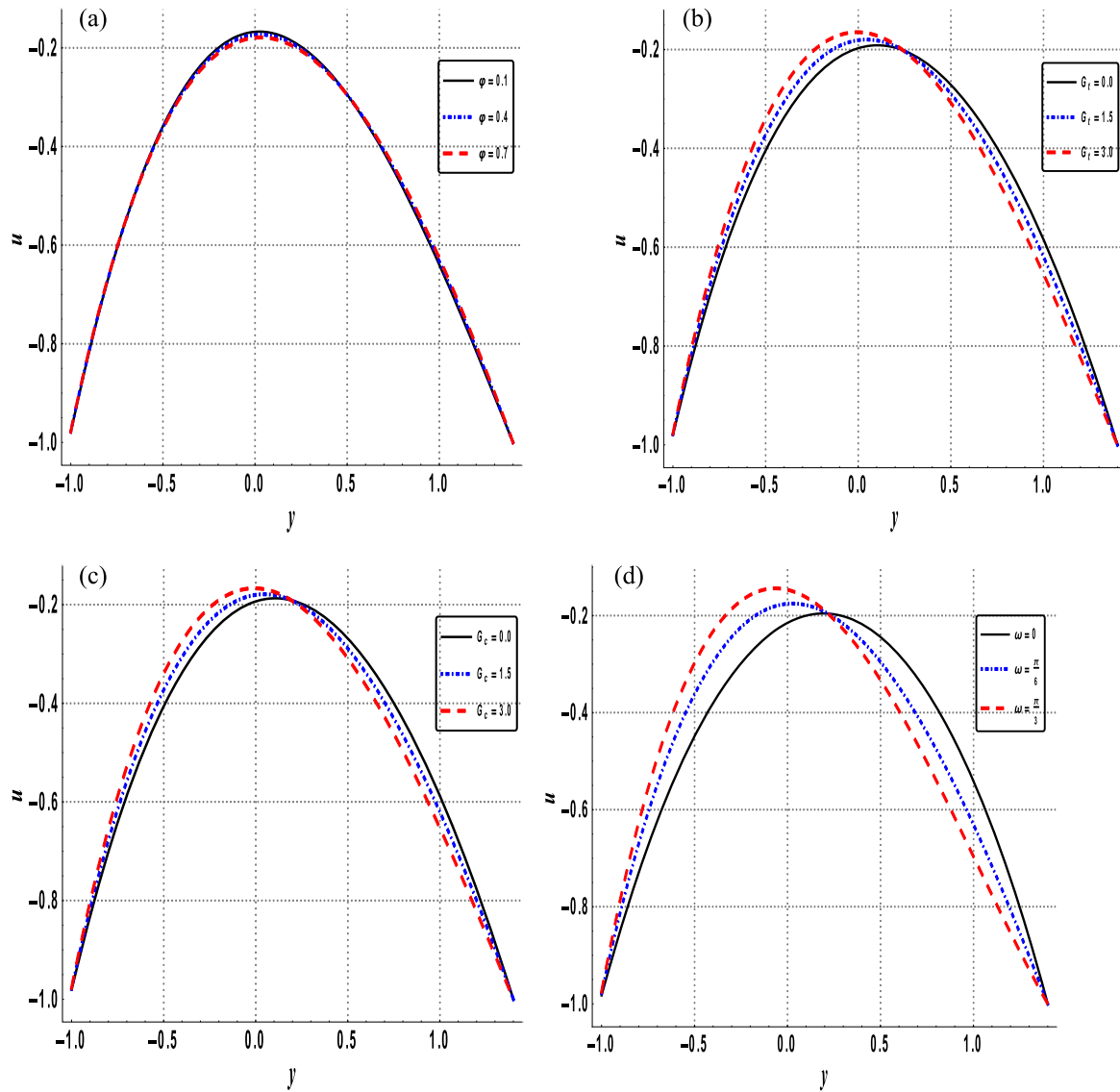
Figure 1. (a)–(d) Variations in velocity when $n = 2.5$, $W_e = 0.1$, $Br = 0.3$, $x = 0$, $Pr = 0.5$, $a = 0.4$, $b = 0.3$, $\mu = 0.7$, $N_t = 0.5$, $N_b = 0.5$, $M = 1$, $G_t = 2.0$, $G_c = 2.0$, $\epsilon = \frac{\pi}{4}$, $d = 0.8$, $\beta = \frac{0.052\,6613}{1.33}$, $\varphi = 0.5$, $\omega = \frac{\pi}{6}$, $\xi = 0.2$.

$$\theta_0 = \frac{h_1 + h_2 - 2y}{2(h_1 - h_2)}, \tag{38}$$

$$\phi_0 = \frac{h_1 + h_2 - 2y}{2(h_1 - h_2)}, \tag{39}$$

The expansion series are defined as:

$$\psi(y, p) = \psi_0 + p\psi_1 + p^2\psi_2 + \ldots, \tag{40}$$

$$\theta(y, p) = \theta_0 + p\theta_1 + p^2\theta_2 + \ldots, \tag{41}$$

$$\phi(y, p) = \phi + p\phi_1 + p^2\phi_2 + \ldots. \tag{42}$$

Using equations (40)–(42) into (31)–(33) and matching the powers of p, the system of linear differential expressions with their relative boundary conditions are solved and as $p \to 1$ solution is obtained as follows:

$$\psi(y) = \psi(y, p)|p \to 1 = \psi_0 + p\psi_1 + p^2\psi_2 + \ldots, \tag{43}$$

$$\theta(y) = \theta(y, p)|p \to 1 = \theta_0 + p\theta_1 + p^2\theta_2 + \ldots, \tag{44}$$

$$\phi(y) = \phi(y, p)|p \to 1 = \phi + p\phi_1 + p^2\phi_2 + \ldots. \tag{45}$$

The zeroth, first and second order systems of linear differential equations are obtained and then solved using computing package in Mathematica. Obtained series solutions are then substituted in equations (43)–(45) to get series expansion of ψ, θ and ϕ. Obtained results are analyzed in next section.

5. Graphical analysis

This section aims to analyze the nature of velocity, entropy, temperature, Bejan number, pressure gradient and concentration through graphs, whereas table 1 is made to examine the heat mass transport rates for different parameters. Present result has been compared with results drawn from
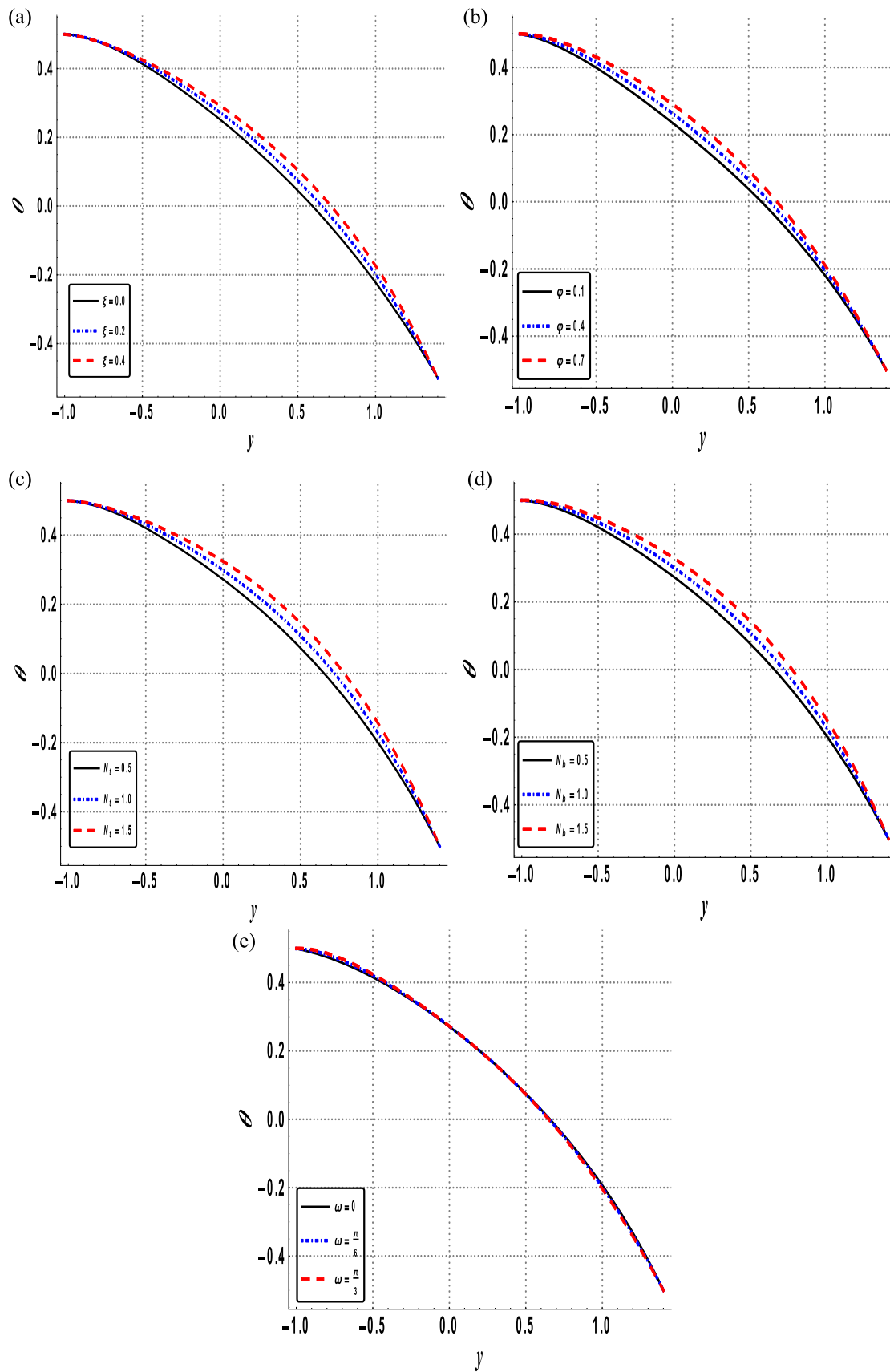
Figure 2. (a)–(e) Variations in temperature when $n = 2.5$, $W_e = 0.1$, $Br = 0.3$, $x = 0$, $Pr = 0.5$, $a = 0.4$, $b = 0.3$, $\mu = 0.7$, $N_t = 0.5$, $N_b = 0.5$, $M = 1$, $G_t = 2.0$, $G_c = 2.0$, $\epsilon = \frac{\pi}{4}$, $d = 0.8$, $\beta = \frac{0.0526613}{1.33}$, $\varphi = 0.5$, $\omega = \frac{\pi}{6}$, $\xi = 0.2$.
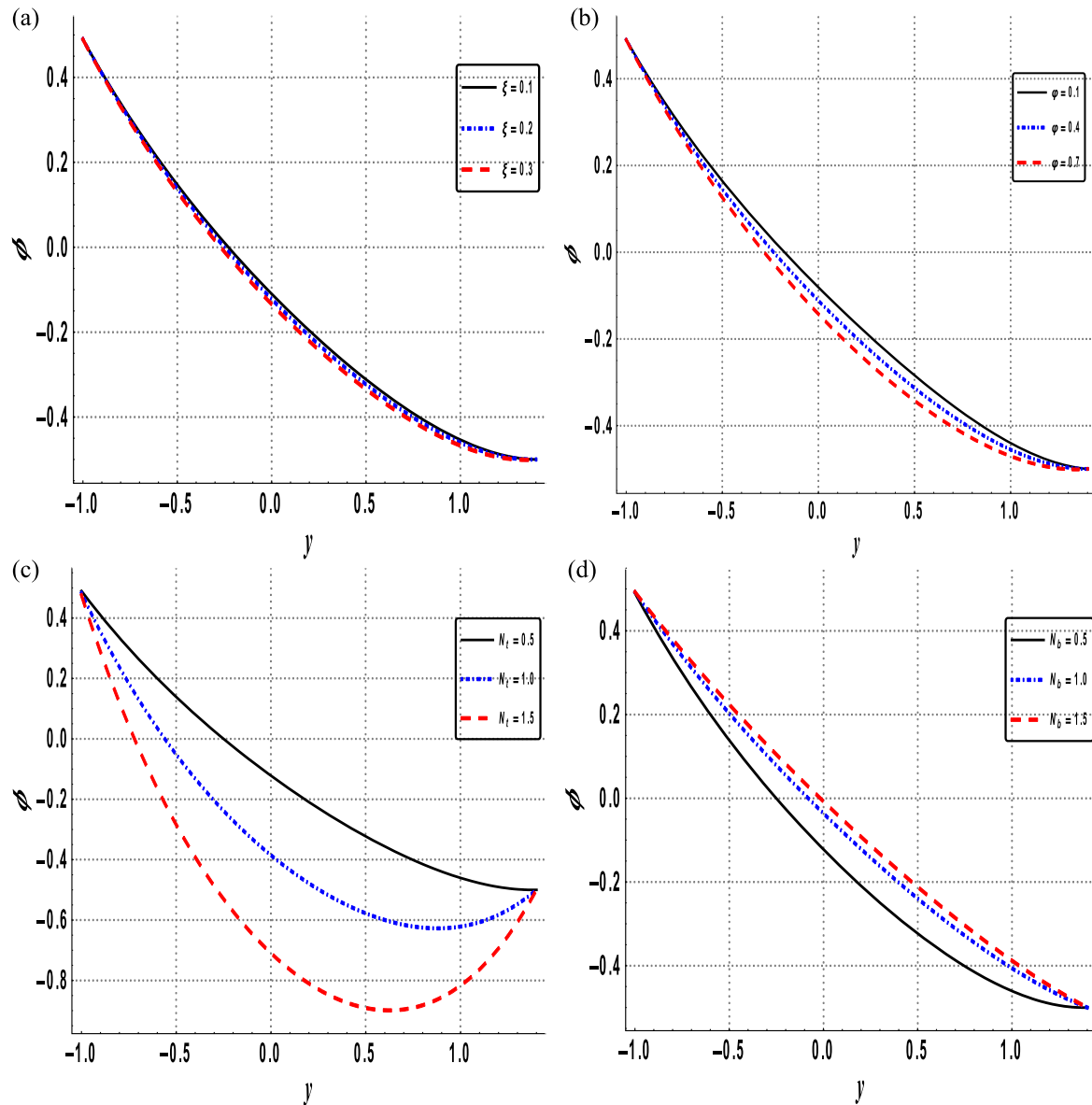
Figure 3. (a)–(d) Variations in concentration when $n = 2.5$, $W_e = 0.1$, $Br = 0.3$, $x = 0$, $Pr = 0.5$, $a = 0.4$, $b = 0.3$, $\mu = 0.7$, $N_t = 0.5$, $N_b = 0.5$, $M = 1$, $G_t = 2.0$, $G_c = 2.0$, $\epsilon = \frac{\pi}{4}$, $d = 0.8$, $\beta = \frac{0.0526613}{1.33}$, $\varphi = 0.5$, $\omega = \frac{\pi}{6}$, $\xi = 0.2$.

numerical approach for its verification. They are in good agreement as they have been illustrated in the figures 8 and 9. To validate current study comparison with other studies given in literature [23] has been presented through table 2. Further, stresses are computed for variation in different parameters.

The variation in velocity profile for various parameters, Hall parameter φ, concentration Grashof number G_c, thermal Grashof number G_t and channel inclination parameter ω are examined through figures 1(a)–(d). All these figures show parabolic path where maximum values are attained near center of channel. Figure 1(a) depicts decreasing behavior with an increment in φ near center of channel but the effects are seen opposite near upper wall. Figure 1(b) shows opposite trend near both walls when G_t is increased i.e. velocity increases when fluid approaches lower wall whereas it is reduced as it approaches upper wall. Similar behavior is seen

for G_c (see figure 1(c)). Figure 1(d) portrays that increase in the values of ω enhances velocity near center of the channel and lower wall, conversely decreasing behavior is observed as it approaches upper wall.

Effects of thermal conductivity ξ, Hall φ, Brownian motion N_b, thermophoresis N_t and channel inclination ω parameters are examined in this section through figures 2(a)–(g). Figures 2(a) and (b) indicate that increase in ξ and φ parameters increase the temperature of fluid. Similar behavior is noticed for both N_t and N_b i.e. temperature increases when these values attain larger values (see figures 2(c) and (d)). Increase in ω near lower wall increases temperature but such increase in ω tends to decrease temperature near upper wall (see figure 2(e)).

Variation in concentration profile for parameters ξ, φ, N_b, and N_t are plotted through figures 3(a)–(d). Figure 3(a) shows that concentration of BN nanoparticles considerably decreases
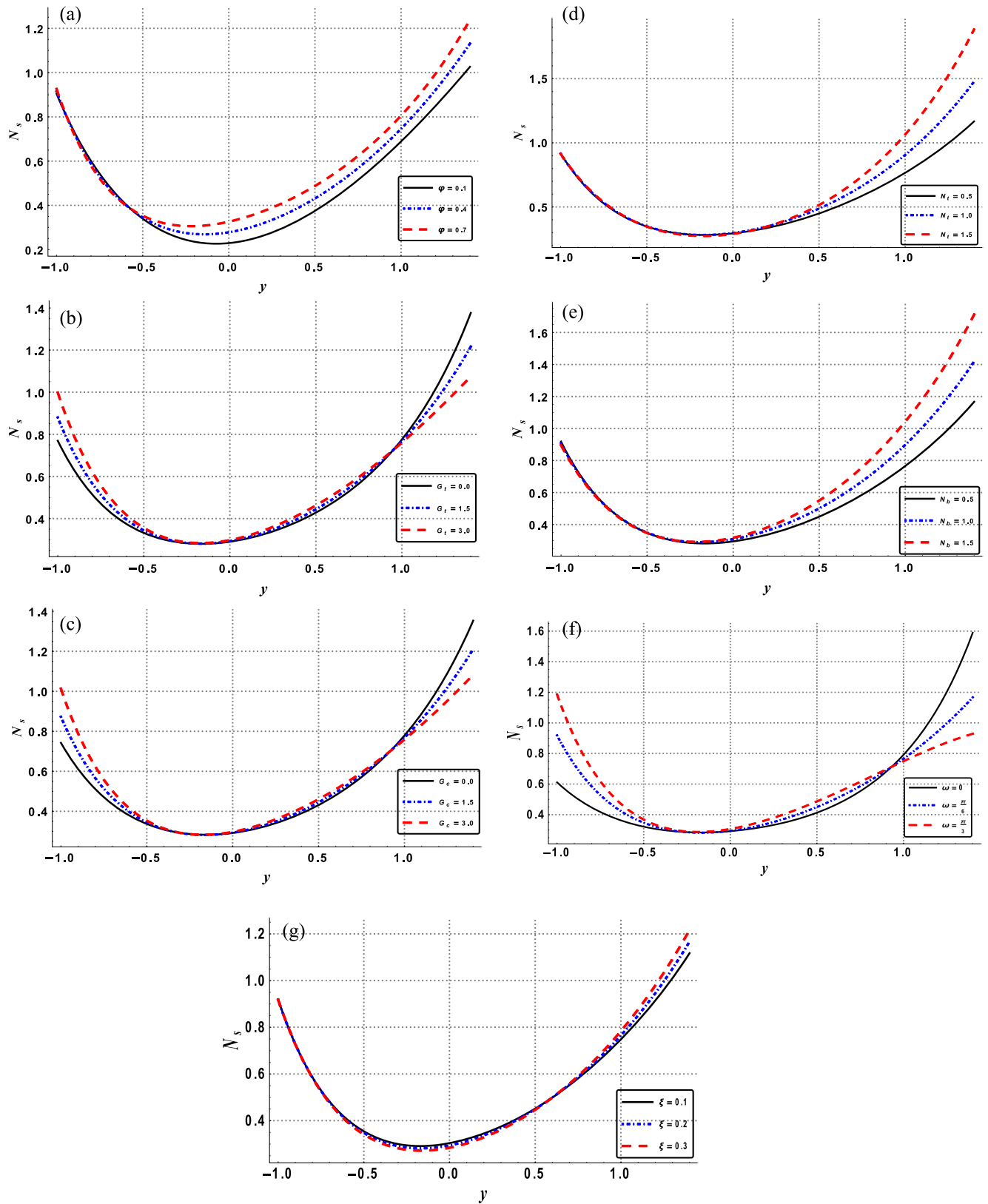
Figure 4. (a)–(g) Variations in entropy generation when $n = 2.5$, $W_e = 0.1$, $Br = 0.3$, $x = 0$, $Pr = 0.5$, $a = 0.4$, $b = 0.3$, $\mu = 0.7$, $N_t = 0.5$, $N_b = 0.5$, $M = 1$, $G_t = 2.0$, $G_c = 2.0$, $\epsilon = \frac{\pi}{4}$, $d = 0.8$, $\beta = \frac{0.0526613}{1.33}$, $\varphi = 0.5$, $\omega = \frac{\pi}{6}$, $\xi = 0.2$.
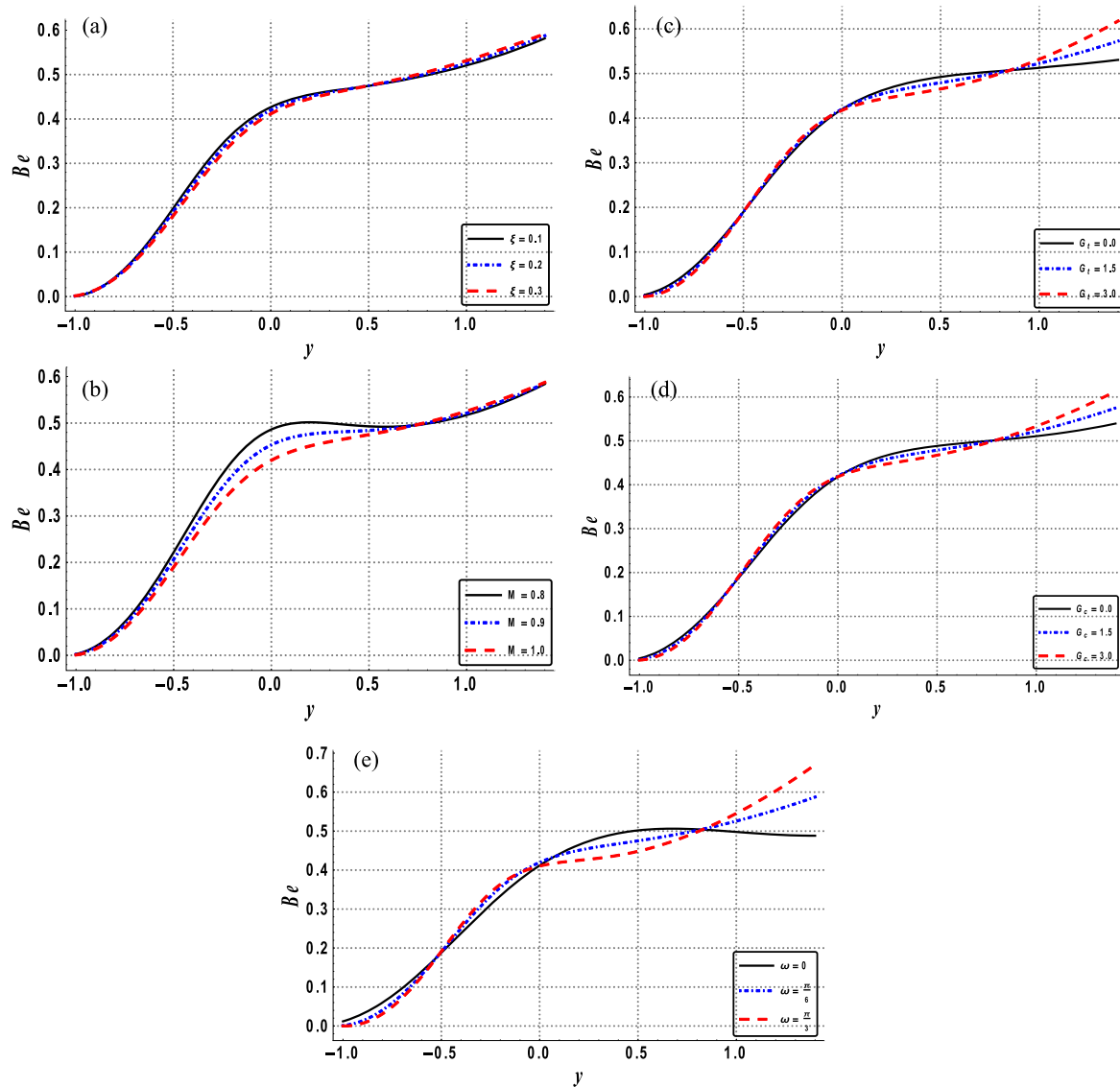
Figure 5. (a)–(e) Variations in bejan number when $n = 2.5$, $W_e = 0.1$, $Br = 0.3$, $x = 0$, $Pr = 0.5$, $a = 0.4$, $b = 0.3$, $\mu = 0.7$, $N_t = 0.5$, $N_b = 0.5$, $M = 1$, $G_t = 2.0$, $G_c = 2.0$, $\epsilon = \frac{\pi}{4}$, $d = 0.8$, $\beta = \frac{0.0526613}{1.33}$, $\varphi = 0.5$, $\omega = \frac{\pi}{6}$, $\xi = 0.2$.

with an increase in ξ. Similarly concentration of nanoparticles can be reduced by increasing the values of φ (see figure 3(b)). Figures 3(c) and (d) notify that the effect of N_t of the concentration nanoparticles is opposite to that of N_b i.e. reduction and enhancement in concentration of nanoparticles is seen for increase in both values of N_t and N_b respectively.

In this section the plots for entropy generation are analyzed in order to explore the effect of various parameters φ, ξ, G_c, N_b, G_t, N_t and ω through figures 4(a)–(g). Figure 4(a) is plotted to check the impact of φ. Significant increase in entropy generation can be noticed for gradual increase in the values of this parameter. Another important point that can be inferred that entropy is greatly affected near the center of the channel. Further, similar behavior is analyzed for both G_t and G_c numbers on entropy generation i.e. it is increased near the center of channel and lower wall, whereas decreased near the channel walls (see figures 4(b)

and (c)). With regard to figures 4(d) and (e) it is observed that entropy generation for N_b and N_t parameters increases as it approaches upper wall. Figure 4(f) shows non uniform behavior of entropy generation under the influence of ω. Noticeable increases in this parameter lead to increase entropy generation near lower wall but decrease near upper wall. This fact depicts that entropy generation can be controlled near upper wall by increasing ω. Also through figure 4(g) it is seen that entropy generation reduces near center of the channel as ξ raises.

Plots for Bejan number are presented to analyze impact of different parameters. Figures 5(a) and (b) show that increase in thermal conductivity parameter ξ and Harman number M, tend to decrease Bejan number while mixed behavior is observed for increase in thermal Grashof number G_t, concentration Grashof number G_c and channel inclination parameter ω through figures 5(c)–(e).
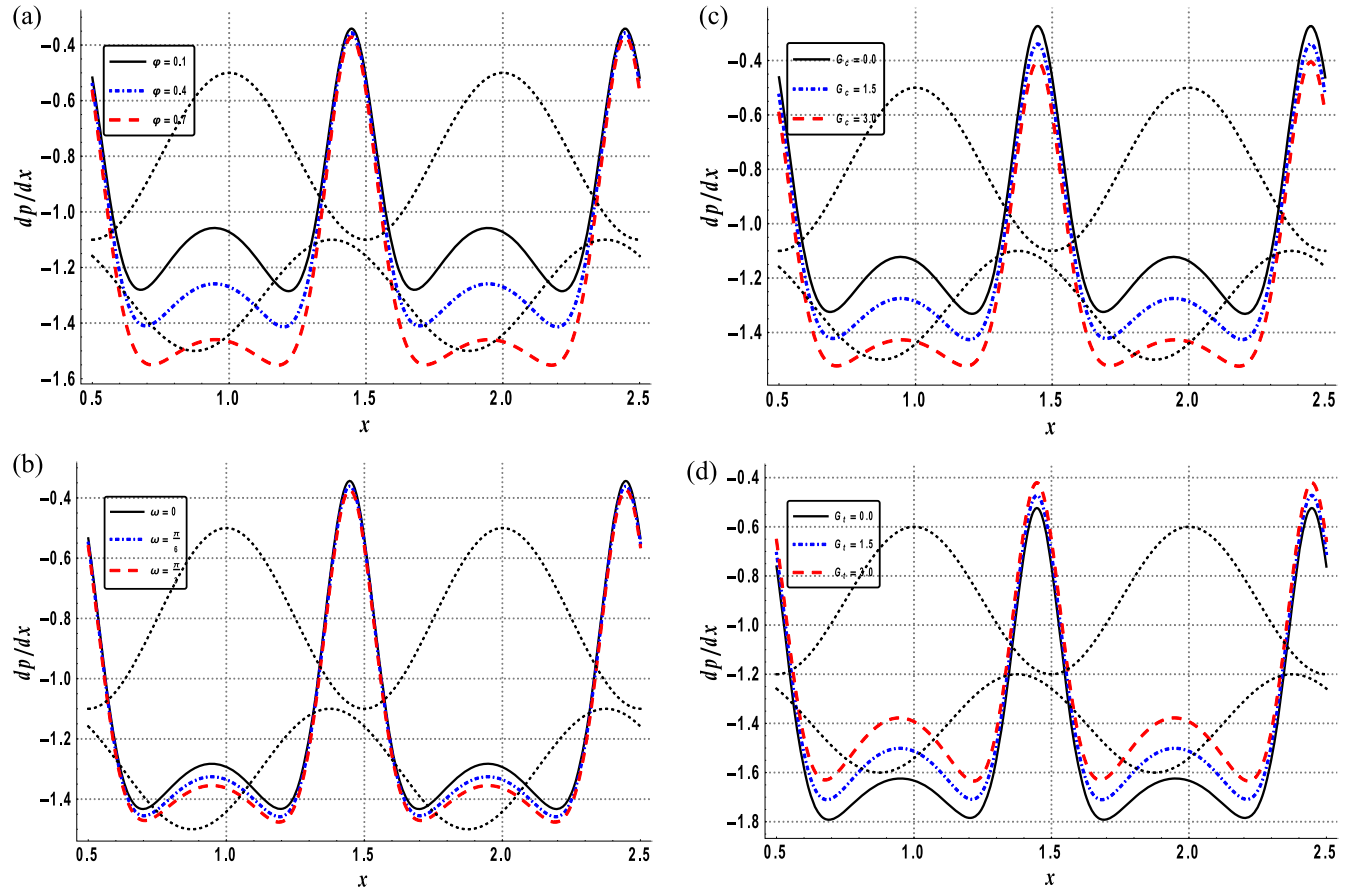
Figure 6. (a)–(d) Variations in pressure when $n = 2.5$, $W_e = 0.1$, $Br = 0.3$, $x = 0$, $Pr = 0.5$, $a = 0.4$, $b = 0.3$, $\mu = 0.7$, $N_t = 0.5$, $N_b = 0.5$, $M = 1$, $G_t = 2.0$, $G_c = 2.0$, $\epsilon = \frac{\pi}{4}$, $d = 0.8$, $\beta = \frac{0.0526613}{1.33}$, $\varphi = 0.5$, $\omega = \frac{\pi}{6}$, $\xi = 0.2$.

The influence of various parameters on pressure gradient is shown in figures 6(a)–(d). Figure 6(a) depicts decreasing behavior for increasing values of Hall parameter φ. Such reduction is large in the wider portion of the channel. Similar reduction is seen for increasing values of both concentration Grashof number G_c and channel inclination parameter ω (see figures 6(b) and (c)). Pressure gradient is minimum in the wider region while it is maximum in the narrow part of the channel. The influence of thermal Grashof number G_t is viewed through figure 6(d) which portrays less enhancement and large enhancement in the contracted and wider parts on the channel respectively.

Bar charts are presented to analyze the impact of Hall parameter φ, channel inclination angle ω, and thermal conductivity parameter ξ through figures 7(a)–(c). There is an enhancement in stress at the wall for increasing values of φ (see figure 7(a)). On the other hand reduction is observed in stresses at the wall for variation in the values of ω and ξ (see figures 7(b)–(c)).

Table 1 is constructed to examine the influence of ξ, φ, G_t, G_c, N_b, N_t and ω on heat and mass transfer rate at the upper wall.

These numerical data depict that increment in the values of φ, ξ, N_b and N_t result in the enhancement in heat transfer rate, whereas such rate reduces with an increase in ω, G_t, and G_c.

Increase in mass transfer can be noticed for increase in N_b. Conversely, enhanced values of N_t, ξ and φ tend to decrease mass transfer rate. Moreover, no change in mass transfer rate is observed for G_t, G_c and ω.

From figures 8 and 9 it is interesting to note that HPM results are in good agreement with the numerical result. Results of study investigated by Abbasi *et al* [23] are showed (see table 2) to observe the validity of found present. Investigators found that more resistance is offered to the fluid due to the increase in effective electric conductivity of nanofluid which heat up the fluid when the hall parameter is increased and, as a result, the temperature increases and both velocity and concentration decrease. This table depicts that present results show qualitative agreement with previously reported results.

6. Conclusions

Entropy generation for MHD mixed convective peristaltic flow of BN-EG nanofluid has been analyzed under the influence of thermophoresis effects and Brownian motion
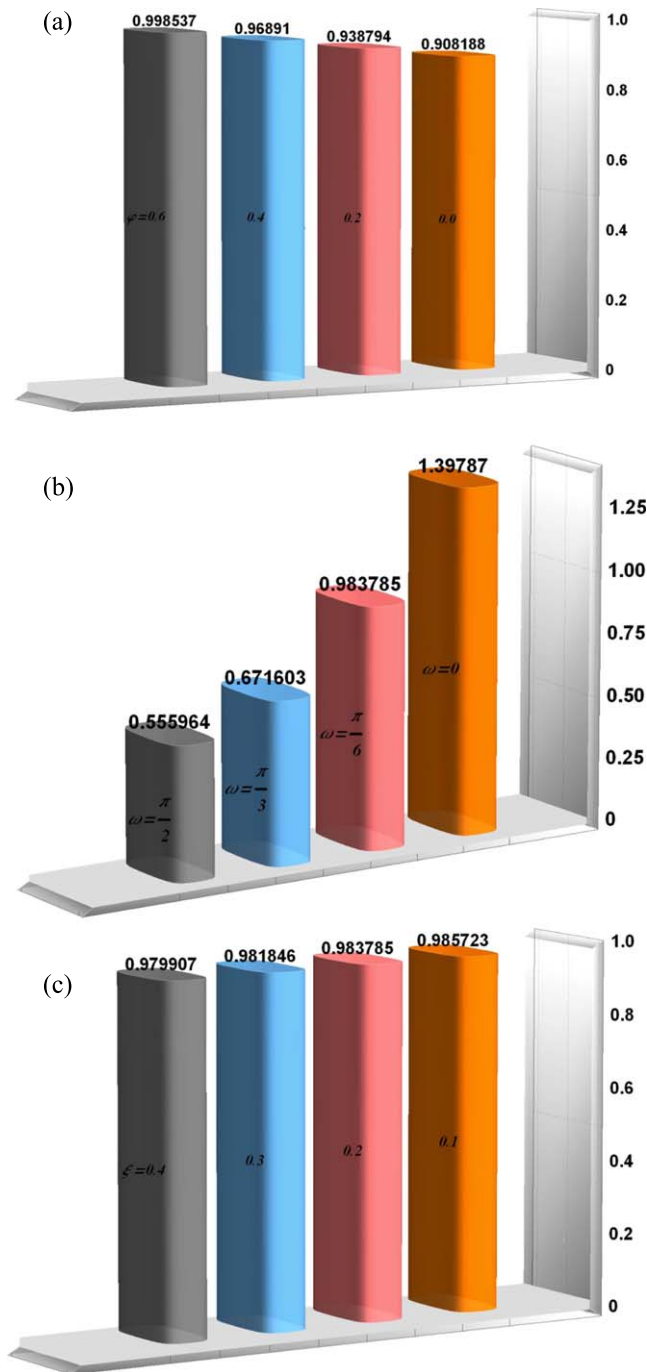
(a)

(b)

(c)

Figure 7. (a)–(c) Variations in stresses when $n = 2.5$, $W_e = 0.1$, $Br = 0.3$, $x = 0$, $Pr = 0.5$, $a = 0.4$, $b = 0.3$, $\mu = 0.7$, $N_t = 0.5$, $N_b = 0.5$, $M = 1$, $G_t = 2.0$, $G_c = 2.0$, $\epsilon = \frac{\pi}{4}$, $d = 0.8$, $\beta = \frac{0.0526613}{1.33}$, $\varphi = 0.5$, $\omega = \frac{\pi}{6}$, $\xi = 0.2$.

with temperature dependent thermal conductivity. Key findings of this analysis are given below:

- Fluid's velocity, concentration of nanoparticles and pressure gradient can be reduced by increasing Hall parameter φ while temperature, heat transfer rate, stress and entropy generation can be increased by increasing φ.
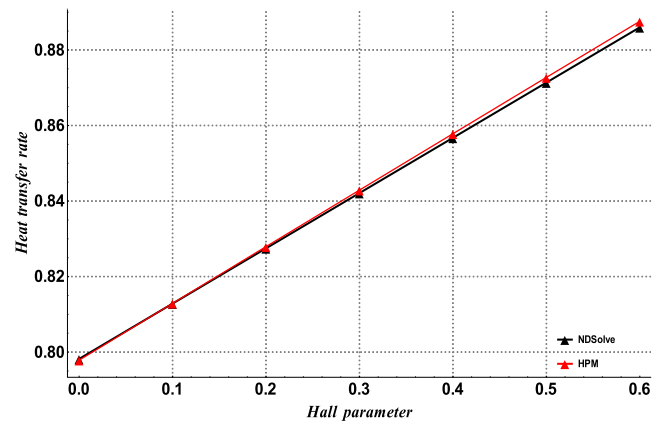

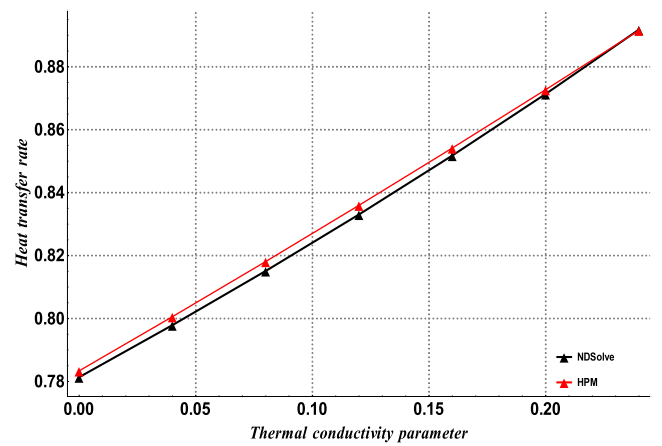**Figure 8.** Comparison of results obtained via different methods.

Figure 9. Comparison of results obtained via different methods.

- Increase in thermal Grashof number G_t, concentration Grashof number G_c and channel inclination parameter ω enhance fluid's velocity but reduce heat transfer rate, entropy near upper wall and pressure gradient.
- Increase in thermal conductivity parameter ξ rises temperature and heat transfer rate while reduces concentration of nanoparticles and stresses in fluid.
- The boosting values of N_b and N_t have opposite effect on mass transfer rate and concentration of BN nanoparticles i.e. increase in N_t and N_b tend to decrease and increase for both profiles.
- Increase in Hartman number M decreases Bejan number near center of the channel.

ORCID iDs

Sabir A Shehzad ⬤ https://orcid.org/0000-0003-3591-9853

References

[1] Choi S U S 1995 Enhancing thermal conductivity of fluids with nanoparticles *ASME Fluids Eng. Div.* **231** 99–105

[2] Wen D and Ding Y 2004 Experimental investigation into convective heat transfer of nanofluids at the entrance region under laminar flow conditions *Int. J. Heat Mass Transfer* **47** 5181–8

[3] Hsiao K 2016 Stagnation electrical MHD nanofluid mixed convection with slip boundary on a stretching sheet *Appl. Therm. Eng.* **98** 850–61

[4] Tabar M A, Alaei M, Khojasteh R R, Motiee F and Rashidi A M 2017 Preference of nano porous graphene to single-walled carbon nanotube (SWCNT) for preparing silica nano hybrid pickering emulsion for potential chemical enhanced oil recovery (C-EOR) *Sci. Iranica* **24** 3491–9

[5] Zhu J, Wang S, Zheng L and Zhang X 2017 Heat transfer of nanofluids considering nanoparticle migration and second-order slip velocity *Appl. Math. Mech.* **38** 125–36

[6] Sheikholeslami M and Shamlooei M 2017 Convective flow of nanofluid inside a lid driven porous cavity using CVFEM *Physica* B **521** 239–50

[7] Sheikholeslami M and Shehzad S A 2018 CVFEM simulation for nanofluid migration in a porous medium using Darcy model *Int. J. Heat Mass Transfer* **122** 1264–71

[8] Sheikholeslami M, Shafee A, Zareei A, Haq R and Li Z 2019 Heat transfer of magnetic nanoparticles through porous media including exergy analysis *J. Mol. Liq.* **279** 719–32

[9] Dogonchi A S, Chamkha A J, Hashemi-Tilehnoee M, Seyyedi S M, Haq R U and Ganji D D 2019 Effects of homogeneous-heterogeneous reactions and thermal radiation on magneto-hydrodynamic Cu-water nanofluid flow over an expanding flat plate with non-uniform heat source *J. Cent. South Univ.* **26** 1161–71

[10] Dogonchi A S, Waqas M and Ganji D D 2019 Shape effects of Copper-Oxide (CuO) nanoparticles to determine the heat transfer filled in a partially heated rhombus enclosure: CVFEM approach *Int. Commun. Heat Mass Transfer* **107** 14–23

[11] Dogonchi A S and Hashim 2019 Heat transfer by natural convection of Fe_3O_4-water nanofluid in an annulus between a wavy circular cylinder and a rhombus *Int. J. Mass Heat Transfer* **130** 320–32

[12] Latham T W 1966 Fluid motion in a peristaltic pump *Master's Thesis* Mass. Inst. Tech, Cambridge

[13] Shapiro A H, Jaffrin M Y and Weinberg S L 1969 Peristaltic pumping with long wavelength at low Reynolds number *J. Fluid Mech.* **37** 799–825

[14] Mishra M and Rao A R 2003 Peristaltic transport of a Newtonian fluid in an asymmetric channel *Z. Angew. Math. Phys.* **54** 532–50

[15] Hayat T, Abbasi F M and Ahmad B 2014 Peristaltic transport of Carreau-Yasuda fluid in a curved channel with slip effects *PLoS One* **4** e95070

[16] Shehzad S A, Abbasi F M, Hayat T and Alsaadi F 2014 MHD mixed convective peristaltic motion of nanofluid with Joule heating and thermophoresis effects *PLoS One* **9** e111417

[17] Abbasi F M, Hayat T and Ahmad B 2015 Peristaltic transport of copper-water nanofluid saturating porous medium *Physica* E **67** 47–53

[18] Tripathi D and Bég O A 2014 A study on peristaltic flow of nanofluids: application in drug delivery systems *Int. J. Heat Mass Transfer* **70** 61–70

[19] Abbasi F M, Shanakhat I and Shehzad S A 2019 Entropy generation analysis for peristalsis of nanofluid with

[20] Żyła G, Witek A and Gizowska M 2015 Rheological profile of boron nitride–ethylene glycol nanofluids *J. Appl. Phys.* **117** 014302

[21] Ellahi R, Aziz S and Zeeshan A 2013 Non-newtonian nanofluid flow through a porous medium between two coaxial cylinders with heat transfer and variable viscosity *J. Porous Media* **16** 205–16

[22] Abbasi F M, Hayat T, Ahmad B and Chen G 2014 Peristaltic motion of a non-newtonian nanofluid in an asymmetric channel *Z. Nat.forsch.* A **69** 451–61

[23] Abbasi F M, Gul M and Shehzad S A 2018 Hall effects on peristalsis of boron nitride-ethylene glycol nanofluid with temperature dependent thermal conductivity *Physica* E **99** 275–84

[24] Zhi C, Xu Y, Bando Y and Golberg D 2011 Highly thermo-conductive fluid with boron nitride nanofillers *ACS Nano* **5** 6571–7

[25] Hayat T, Nawaz S, Alsaedi A and Rafiq M 2016 Analysis of entropy generation in mixed convective peristaltic flow of nanofluid *Entropy* **18** 355

[26] Hakeem A K A, Govindaraju M, Ganga B and Kayalvizhi M 2016 Second law analysis for radiative MHD slip flow of a nanofluid over a stretching sheet with non-uniform heat source effect *Sci. Iranica* **23** 1524–38

[27] Ghaffarpasand O 2017 Natural convection and entropy generation of ultrafine atmospheric aerosols in the presence of hydrodynamic partial slip and thermal radiation due to solar energy *Sci. Iranica* **24** 1686–705

[28] Li Z, Sheikholeslami M, Jafaryar M, Shafee A and Chamkha A J 2018 Investigation of nanofluid entropy generation in a heat exchanger with helical twisted tapes *J. Mol. Liq.* **266** 797–805

[29] Abbasi F M, Shanakhat I and Shehzad S A 2019 Entropy generation analysis in peristalsis of nanofluid with Ohmic heating and Hall effects *Phys. Scr.* **94** 025001

[30] Sheikholeslami M 2019 New computational approach for exergy and entropy analysis of nanofluid under the impact of Lorentz force through a porous media *Comput. Methods Appl. Mech. Eng.* **344** 319–33

[31] Nguyen T Y, Sheikholeslami M, Shehzad S A, Shafee A and Alghamdi M 2019 Solidification entropy generation via FEM through a porous storage unit with applying magnetic field *Phys. Scr.* **94** 095207

[32] Seyyedi S M, Dogonchi A S, Ganji D D and Hashemi-Tilehnoee M 2019 Entropy generation in a nanofluid-filled semi-annulus cavity by considering the shape of nanoparticles *J. Therm. Anal. Calorim.* **138** 1607–21

[33] Seyyedi S M, Dogonchi A S, Ganji D D, Nuraei R and Hashemi-Tilehnoee M 2019 Numerical analysis of entropy generation of a nanofluid in a semi-annulus porous enclosure with different nanoparticle shapes in the presence of a magnetic field *Eur. Phys. J. Plus* **134** 268

[34] Seyyedi S M, Dogonchi A S, Hashemi-Tilehnoee M, Asghar Z, Waqas M and Ganji D D 2019 A computational framework for natural convective hydromagnetic flow via inclined cavity: an analysis subjected to entropy generation *Journal of Molecular Liquids* **287** 110863